Dalton Transactions

Composition-defined Nanosized Assemblies that Contain Heterometallic Early 4d/5d-Transition-Metals

Journal:	*Dalton Transactions*
Manuscript ID	DT-ART-07-2019-003094
Article Type:	Paper
Date Submitted by the Author:	29-Jul-2019
Complete List of Authors:	Wakizaka, Masanori; Tokyo Institute of Technology Imaoka, Takane; Tokyo Institute of Technology, Chemical Resources Laboratory Yamamoto, Kimihisa; Tokyo Institute of Technology, Chemical Resources Laboratory

ARTICLE

Composition-defined Nanosized Assemblies that Contain Heterometallic Early 4d/5d-Transition-Metals

Received 00th January 20xx,
Accepted 00th January 20xx

DOI: 10.1039/x0xx00000x

Masanori Wakizaka,[a] Takane Imaoka,*[,a] and Kimihisa Yamamoto*[,a]

The controlled assembly of the early transition metals remains a challenging research target, especially with respect to the generation of heterometallic molecules and nanomaterials. In this study, metal chlorides of the early 4d/5d-transition-metals, *i.e.*, $ZrCl_4$, $NbCl_5$, $MoCl_5$, $HfCl_4$, $TaCl_5$, and WCl_6, were stoichiometrically introduced into a tetraphenylmethane-core dendritic-phenylazomethine generation 4 dendrimer in the presence of an optimal amount of organic ligands such as pyridine and 3-chloropyridine. The coordinative interactions between the metal chlorides and the imines in the dendrimers indicated a positive correlation for the Lewis acidity of the metals. Moreover, it was clearly demonstrated for the first time that heterometallic assemblies of defined composition contain four kinds of early 4d/5d-transition-metals, such as Ta^{V}, Nb^{V}, Mo^{V}, and Zr^{IV}, which was confirmed by UV-vis titration, XPS, and HAADF-STEM/EDS measurements. The results of this study should open new access routes to nanomaterials composed of the heterometallic early 4d/5d-transition metals.

Introduction

Early transition metals (group IV-VI) represent some of the most desirable elements for the production of unique assembly structures such as multinuclear metal complexes,[1,2] polyoxometalates,[3] clusters,[4] and nanoparticles,[5] mostly due to the fact that these elements can easily access a wide range of oxidation states and bonding modes.[6] Moreover, it was reported that mixing of different kinds of the early transition metals modulated redox,[7] catalytic,[8] or photochemical properties,[9,10] for example. Thus, the controlled assembly of such metals has been an attractive research target.[7–15] In this context, heterometallic multinuclear complexes and clusters that involve three different early transition metals, such as $[CrMoW(2,2'\text{-dipyridylamide})_4Cl_2]$,[7] $[Zr(C_5H_5)_2\{NbO(\alpha\text{-}PW_{11}O_{39})\}_2]^{6-}$,[13] or $Ta_nNb_mM_k^{+}$ (M = V, Mo, W)[15] were reported by Berry *et al.*, Beer *et al.*, and Mafuné *et al.*, respectively. These studies clearly demonstrated that it is possible to generate new heterometallic molecules and nanomaterials that contain more than two different types of early transition metals, although the assemblies of four or more different types of the early transition metals still remain elusive.

Dendrimers, on the other hand, are repetitively branched macromolecules that exhibit monodispersed compositions, multi-layer structures, and an internal space.[16,17] Based on their characteristics, dendrimers are suitable as molecular templates for the construction of macromolecular complexes in order to assemble metals, which allows the synthesis of nanoparticles,[18–20] as well as host molecules for nanosized assemblies.[21–31] Especially, dendritic-phenylazomethine (DPA) dendrimers exhibit unique coordination behavior, as the basicity gradients induced by the electrostatic potential gradients on the individual imine sites results in a stepwise radial assembly pattern of the metals on each imine site (Figure 1).[32–37] This property affords control over the composition of the resulting heterometallic macromolecular complexes and the size of the corresponding nanoparticles.[32–39] For instance, the combinations of Fe^{III}/Sn^{II} [38] or $Au^{III}/Pt^{IV}/Cu^{II}$ [39] metals have been reported to assemble in DPA dendrimers in a particular fashion. DPA dendrimers might potentially act as universal molecular templates for the creation of ultrasmall nanomaterials. On the other hand, the stepwise radial assembling of the early transition metals into DPA dendrimers remains to be accomplished,[40] probably due to the high Lewis acidity of the early transition metals.[41] Therefore, the development of a

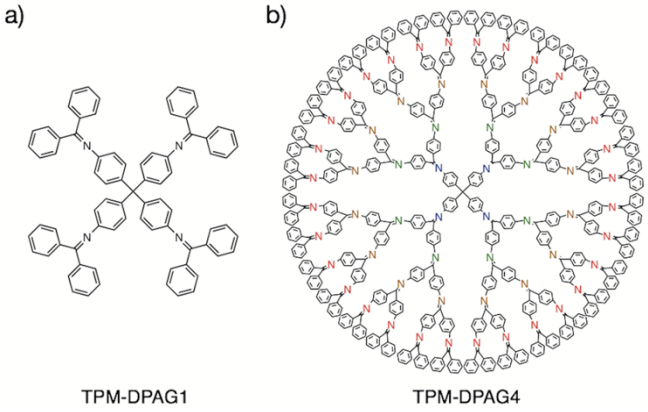

Figure 1. Molecular structures of TPM-DPA dendrimers of a) G1 and b) G4.

[a] *Laboratory for Chemistry and Life Science Institute of Innovative Research, Tokyo Institute of Technology, Yokohama 226-8503, Japan*
† Correspondence and requests for materials should be addressed to K.Y. E-mail: yamamoto@res.titech.ac.jp
Electronic Supplementary Information (ESI) available: UV-vis spectral changes of TPM-DPAG1 and G4, fitting curves, equation for the equilibrium constant, ^{1}H NMR spectra, a representative illustration for the coordination models, and XPS and EDS data are listed in the supporting information. See DOI: 10.1039/x0xx00000x

systematic method to assemble such metals in a DPA dendrimer is highly desirable for the generation of new assemblies that contain early transition metals.

In this study, we developed a method for the generation of heterometallic assemblies that incorporate heterometallic early transition metals. For that purpose, we examined the interactions between the DPA dendrimers and the early 4d/5d-transition metals, *i.e.*, Zr^{IV}, Nb^{V}, Mo^{V}, Hf^{IV}, Ta^{V}, and W^{VI}. Moreover, we systematically assembled these metals into the tetraphenylmethane-core DPA generation 4 dendrimer (TMP-DPAG4) in the presence of an optimal amount of organic ligands, which produced the first examples of composition defined heterometallic assemblies that involve Ta, Nb, Mo, and Zr.

Experimental

Materials

TPM-DPAG1 and G4 were prepared according to previously reported procedures.[42,43] $ZrCl_4$, $MoCl_5$, $HfCl_4$, WCl_6, 3-chloropyridine (3-Clpy), hexamethylphosphoramide (HMPA), and graphitized mesoporous carbon (GMC) were purchased from Sigma-Aldrich. $NbCl_5$ and $TaCl_5$ were purchased from Alfa Aesar. Dehydrated dichloromethane (CH_2Cl_2), dehydrated tetrahydrofuran (THF), dehydrated *n*-hexane, dehydrated pyridine (py), methanol (MeOH), and molecular sieves 3A (MS3A) were purchased from Kanto Chemical Co., Inc. Prior to use, MS3A was washed with tap water and distilled water before being dried at 373 K for more than 24 h hours *in vacuo*. All the solvents were treated with MS3A for further dehydration, and THF was distilled from Na-benzophenone ketyl prior to use. The GMC was washed with distilled water and MeOH, followed by filtration and drying *in vacuo*. Subsequently, the GMC was heated for 3 h to 1173 K under a flow (500 mL min^{-1}) of H_2 (3%) in Ar.

Titration Experiments

3000 μL CH_2Cl_2/THF = 2/1 (*v*/*v*) solutions of TPM-DPAG1 (9.0 μM) or TPM-DPAG4 (3.0 μM) in the presence of defined amounts of py, 3-Clpy, and/or HMPA were prepared in an optical quartz cell (optical path = 1.0 cm) under an atmosphere of dry N_2 (~1 ppm water and oxygen) at 245 K. Subsequently, defined amounts of the THF solutions of the metal salts were added to the solution using a micropipette.

Preparation of the samples

The heterometallic assembly sample. 3000 μL pale yellow CH_2Cl_2/THF = 2/1 (*v*/*v*) solution of TPM-DPAG4 (3.0 μM) in the presence of py (14 eq.) and 3-Clpy (240 eq.) was prepared under an atmosphere of dry Ar at 245 K. Subsequently, the THF solutions of $TaCl_5$ (4 eq.), $NbCl_5$ (8 eq.), $MoCl_5$ (16 eq.), and $ZrCl_4$ (32 eq.) were added to the solution. After stirring for 45 min at 245 K, the solution turned deep yellow. Then, the solution was dropped with stirring into the GMC (4.5 mg) suspension in CH_2Cl_2 (1000 μL), which was dispersed under sonication for 2 min. After filtration, the powder sample was washed with *n*-hexane (2 × 1000 μL) and dried *in vacuo* for 2 h.

The crude mixture sample for XPS. $TaCl_5$ (14.5 mg, 40.5 mmol), $NbCl_5$ (12.2 mg, 45.2 mmol), $MoCl_5$ (11.4 mg, 41.7 mmol), and $ZrCl_4$ (10.7 mg, 45.9 mmol) were grided and mixed in an agate mortar under an atmosphere of dry Ar. Then, the mixture of the metal chlorides (2.0 mg) and the GMC (6.0 mg) were mixed in the same way, afforded the crude mixture sample.

The crude mixture sample for HAADF-STEM/EDS. THF solutions (3 mM) of $TaCl_5$ (0.36 mmol), $NbCl_5$ (0.72 mmol), $MoCl_5$ (1.44 mmol), and $ZrCl_4$ (2.88 mmol) were added to the GMC (4.5 mg) under an atmosphere of dry Ar. The suspension was stirred for 5 min, then dispersed under sonication for 2 min. Following evaporation, the powder sample was dispersed in *n*-hexane (4000 μL), filtered, washed with *n*-hexane (2 × 1000 μL), and dried *in vacuo* for 2 h.

The Mo assembly sample. 3000 μL pale yellow CH_2Cl_2/THF = 2/1 (*v*/*v*) solution of TPM-DPAG4 (3.0 μM) in the presence of py (4 eq.) and 3-Clpy (40 eq.) was prepared under an atmosphere of dry Ar at 245 K. Subsequently, the THF solutions of $MoCl_5$ (60 eq.) was added to the solution. After stirring for 45 min at 245 K, the solution turned deep yellow. Then, the solution was dropped with stirring into the GMC (9.0 mg) suspension in CH_2Cl_2 (1000 μL), which was dispersed under sonication for 2 min. After filtration, the powder sample was washed with *n*-hexane (2 × 1000 μL) and dried *in vacuo* for 2 h.

Measurements

The UV-vis spectra were recorded by a Shimadzu UV-2700 spectrophotometer at 245 K in a glove box under an atmosphere of dry N_2. The ^1H NMR spectra were recorded by a Bruker AVANCE III (400 MHz) spectrometer. The X-ray photoelectron spectroscopy (XPS) measurements were performed using an ESCA 1700R ULVAC-PHI, and the binding energy was calibrated using C1s (284.5 eV) as the reference. High-angle annular dark-field scanning transmission electron microscopy (HAADF-STEM) and energy dispersive X-ray spectrometry (EDS) analyses were performed by a JEOL JEM-ARM200F ACCELARM (accelerating voltage = 80 kV) with Cs-corrector and silicon drift detectors (2 × 100 cm^2). The analytes in an *n*-hexane suspension were dropped onto micro Cu grids with carbon filaments (Alliance Biosystems thin holey carbon film coated grids), and dried for > 12 h *in vacuo* at r.t.

Results and discussion

Complexation of Early 4d/5d-transition Metals

Figure 2a shows the UV-vis spectral change of TPM-DPAG1 during the titration with 300 eq. of HMPA in CH_2Cl_2/THF = 2/1(*v*/*v*) at 245 K. The TPM-DPAG1 showed absorption bands at 253 and 348 nm, both of which involve conjugated π-π* transition bands.[32–40] The addition of $TaCl_5$ (0.5-5.5 eq.) induced spectral changes with an isosbestic point at 279.0 nm, suggesting complexation between Ta^{V} and the imines in TPM-DPAG1.[32–40] As the spectral change did not reach saturation

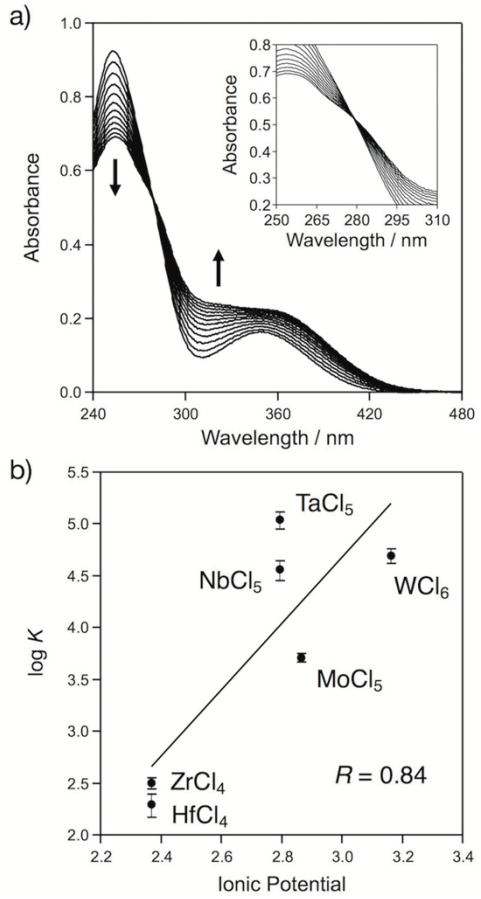

Figure 2. a) Full range (240–480 nm) UV-vis spectral change of TPM-DPAG1 in CH_2Cl_2/THF = 2/1(*v*/*v*) upon the addition of $TaCl_5$ (0, 0.5, 1, 1.5, 2, 2.5, 3, 3.5, 4, 4.5, 5, and 5.5 eq.) in the presence of HMPA (300 eq.) under an atmosphere of N_2 at 245 K. The insert is magnification around the isosbestic point (250–310 nm). b) Relationship between the ionic potential of metals and log *K* of TPM-DPAG1 and metal chlorides together with the correlation coefficient (*R*).

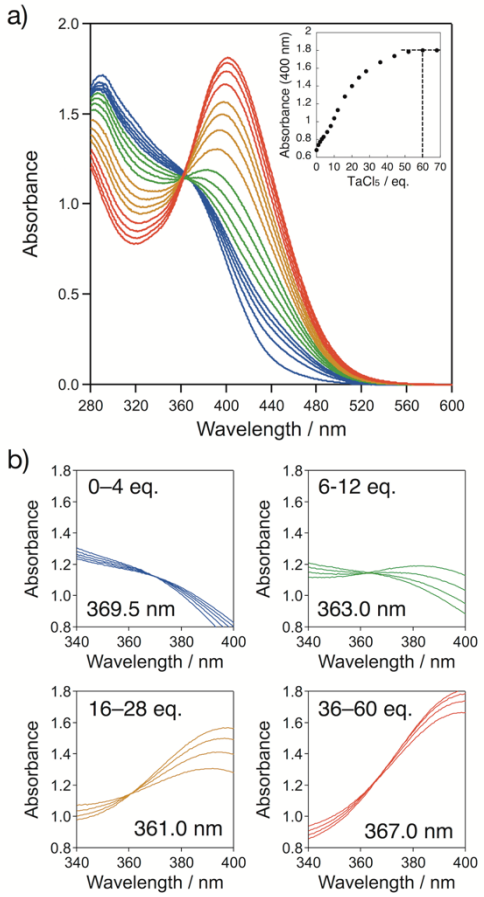

Figure 3. a) Full range (280–600 nm) and b) magnifications around the isosbestic points (340–400 nm) of the UV-vis spectral change of TPM-DPAG4 in CH_2Cl_2/THF = 2/1(*v*/*v*) upon the addition of $TaCl_5$ (0, 1, 2, 3, and 4 eq.; blue lines), (6, 8, 10, and 12 eq.; green lines), (16, 20, 24, and 28 eq.; orange lines), and (36, 44, 52, and 60 eq.; red lines) in the presence of py (20 eq.) and 3-Clpy (600 eq.), under an atmosphere of N_2 at 245 K.

upon addition of 4 eq. of $TaCl_5$ despite the presence of four imines in TPM-DPAG1, the interaction seems to be moderate under these conditions and involve an excess of HMPA.[44] Under similar conditions, the addition of other metal chlorides, *i.e.*, $NbCl_5$, $MoCl_5$, $HfCl_4$, $TaCl_5$, or WCl_6, indicated similar spectral changes (Figure S1), suggesting complexation between TPM-DPAG1 and these metals. These spectra showed the comparable maximum absorption wavelengths (~253 nm), which suggests that the electrostatic interactions between the imines and these metals are dominant. However, the equilibrium constants (*K*) between the imines in TMP-DPAG1 and the metal chlorides, were determined on the basis of the curves fitting of the equilibrium with an equimolar metal/imine ratio (Figure S2 and Equation S1)[45] which were clearly different: $1.1\pm0.2 \times 10^5$ ($TaCl_5$), $5.0\pm0.8 \times 10^4$ (WCl_6), $3.7\pm0.8 \times 10^4$ ($NbCl_5$), $5.2\pm0.5 \times 10^3$ ($MoCl_5$), $3.2\pm0.4 \times 10^2$ ($ZrCl_4$), and $2.0\pm0.5 \times 10^2$ M^{-1} ($HfCl_4$). The relationship between the ionic potential $(Z/r)^{1/2}$,[46] whereby *Z* is the charge of the metal and *r* the ionic radius of the metal,[47] and log *K* of TPM-DPAG1 and the metal chlorides (Figure 2b) indicated a positive correlation (*R* = 0.84), supported by the electrostatic interactions between the imines and these metals.

Systematic Assembly of Early 4d/5d-transition Metals

The UV-vis spectrum of TPM-DPAG4 in CH_2Cl_2/THF = 2/1(*v*/*v*) at 245 K exhibited absorption bands at 290 nm accompanied by a shoulder at 370 nm (Figure S3). The addition of $TaCl_5$ afforded a spectral change accompanied by a decrease and increase of the absorbance at ~280 and ~400 nm, respectively (Figure S3e). This spectral change should correspond to the complexation between Ta^V and the imines of TPM-DPAG4, since the spectral change resembles those of previous reported metals such as $SnCl_2$.[32–40] Whereas addition of $SnCl_2$ afforded stepwise shifts in the isosbestic points based on the stoichiometric coordinations between Sn^{II} and the imines in the DPA dendrimer,[32] the addition of $TaCl_5$ did not show any clear isosbestic points. Moreover, the spectral change was saturated upon the addition of *ca*. 12 eq. of $TaCl_5$, even though TPM-DPAG4 contains 60 imine sites in total. The saturation amounts were different, however this nonstoichiometric coordination behavior was also observed upon the addition of $ZrCl_4$, $NbCl_5$, $MoCl_5$, $HfCl_4$, or WCl_6 (Figures S3a-S3d and S3f). A negative relationship was observed between log *K* and the saturation amount of the metal chlorides at *R* = 0.98 (Figure S4). Accordingly, stronger

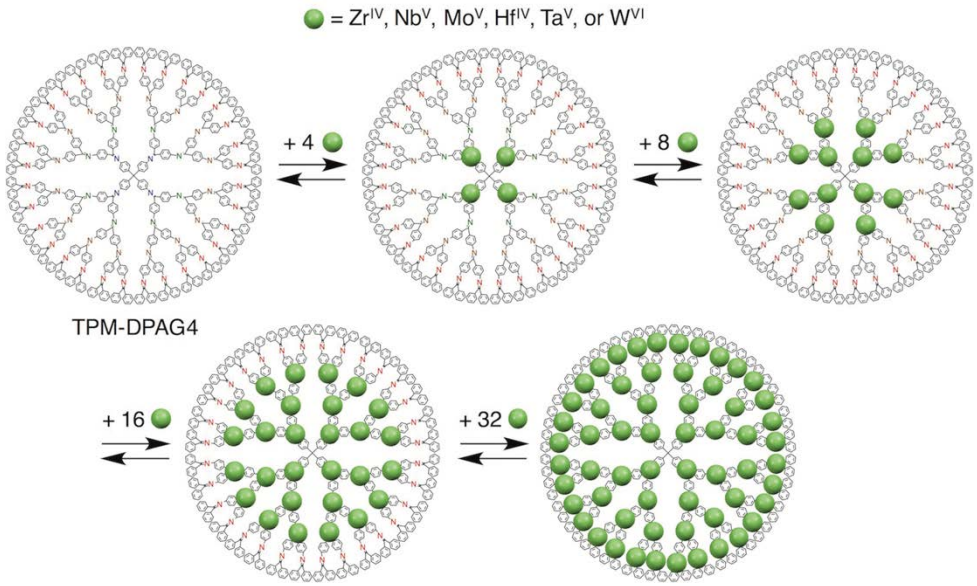

Scheme 1. A plausible scheme for stepwise radial assembling of early 4d/5d-transition metals in TPM-DPAG4.

interactions should prevent a stoichiometric coordination between the metals and the imines. A multidentate by the imines in the TPM-DPAG4 would be a reasonable model, which saturates with substoichiometric amounts of metals relative to the number of imine moieties (Figure S5).[48,49]

In order to inhibit the multidentate, further titration experiments were carried out in the presence of base additives such as py and 3-Clpy. As the result of the titration in the presence of py (20 eq.) and 3-Clpy (600 eq.), the UV-vis spectral change was saturated upon the addition of 60 eq. of $TaCl_5$ (Figure 3), suggesting stoichiometric coordination between Ta^{V} and the imines. In addition, the addition of 1-4 eq. of $TaCl_5$ afforded a spectral change that produced an isosbestic point at 369.5 nm. Moreover, during the addition of 6-12, 16-28, and 36-60 eq. of $TaCl_5$, the isosbestic points shifted to 363.0, 361.0, and 367.0 nm, respectively, before the spectral change was saturated upon the addition of 60 eq. of $TaCl_5$. Since TPM-DPAG4 contains 4, 8, 16, and 32 imines from the inner sites towards to the periphery, respectively, the shifts in the isosbestic point suggests that the Ta^{V} are stoichiometrically coordinated by the imines in a stepwise fashion from the inner sites towards to the periphery (Scheme 1).[32–40] The driving force of the stepwise radial assembling in the DPA dendrimers was proposed based on the basicity gradient for each imine site.[32–40] Similar spectral changes and shifts in the isosbestic point were observed upon the addition of $ZrCl_4$, $NbCl_5$, $MoCl_5$, $HfCl_4$, or WCl_6 (Figures S6-S10) in the presence of defined amounts of py and 3-Clpy, indicating a stoichiometric and stepwise radial coordination. Py (pK_b = 12.6) and 3-Clpy (pK_b = 10.0) coordinate to metals in the solution and/or in TPM-DPAG4,[50] and thus prevent a multidentate between the metals and the imines. The optimal amount of py and 3-Clpy was positively correlated with the ionic potential of the metals (R = 0.96 and 0.99) except for Mo^{V} (Figure S11), suggesting that required amount of base for the stepwise radial assembling is determined by the ionic potential of metals in the case of d^0 electronic configuration. On the other hand, Mo^{V} (d^1) deviated from the correlation, as the d^1 metals could be stabilized not only by the electrostatic interaction with py and 3-Clpy but also by the back-donative interaction with them. It is noteworthy that the coordination of py and 3-Clpy is supported by the downfield shifts of the ^{1}H NMR signals of both the imines and py or 3-Clpy upon the addition of $TaCl_5$ (Figures S12), for example.

Heterometallic Assembly of Early 4d/5d-Transition-Metals

It has been reported that metals that exhibit a stronger Lewis acidity selectively coordinate to the imines on the inner sites of the DPA dendrimers, whereas metals with lower K values selectively coordinate to those of the outer sites.[36,38,39] As Ta^{V}, Nb^{V}, Mo^{V}, and Zr^{IV} exhibit a relatively strong Lewis acidity in this context (Figure 2b), these metals should assemble on each site in the TPM-DPAG4. Figure 4 shows the UV-vis spectral changes in CH_2Cl_2/THF = 2/1(v/v) at 245 K upon the continuous addition of $TaCl_5$, $NbCl_5$, $MoCl_5$, and $ZrCl_4$. The addition of $TaCl_5$ (1-4 eq.) afforded the characteristic spectral change corresponding to the coordination on the imines with an isosbestic point at 368.0 nm. The subsequent addition of $NbCl_5$ (2-8 eq.), $MoCl_5$ (4-16 eq.), and $ZrCl_4$ (8-32 eq.) showed shifts in the isosbestic points to 362.5, 364.5, and 362.0 nm, respectively. In addition, the spectral change saturated upon the addition of a total of 60 eq. of the metal chlorides. Theses spectral changes thus suggest that Ta^{V} (4 eq.), Nb^{V} (8 eq.), Mo^{V} (16 eq.), and Zr^{IV} (32 eq.) were stoichiometrically coordinated in a stepwise fashion to the imines in TPM-DPAG4 (Scheme 2).[36,38,39]

In order to reveal the composition of the heterometallic assembly composed of $M^{n+}Cl_n$ (M = Ta^{V}, Nb^{V}, Mo^{V}, Zr^{IV}) and TPM-DPAG4, the XPS spectra of the assembly supported on the GMC were recorded (Figure 5). The paired peaks appeared at 26.5/28.3, 207.8/210.6, 232.2/235.5, and 183.4/185.7 eV, and are assigned to Ta^{V}, Nb^{V}, Mo^{V}, and Zr^{IV}, respectively, based on the comparison with the crude mixture of their metal chlorides on the GMC (Figure S13 and Table S1). We also estimated the

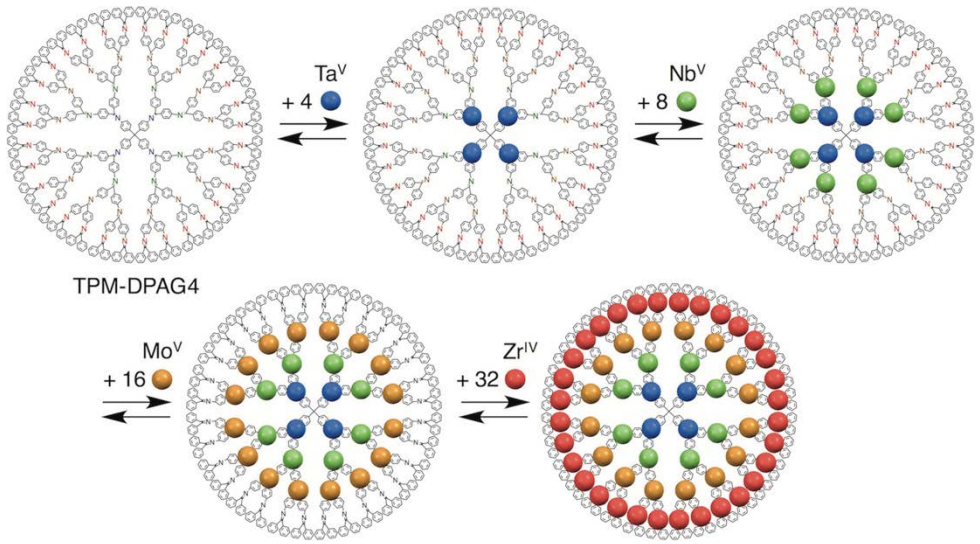

Scheme 2. A plausible scheme for stepwise and radial assembling of four different early 4d/5d-transition metals in TPM-DPAG4.

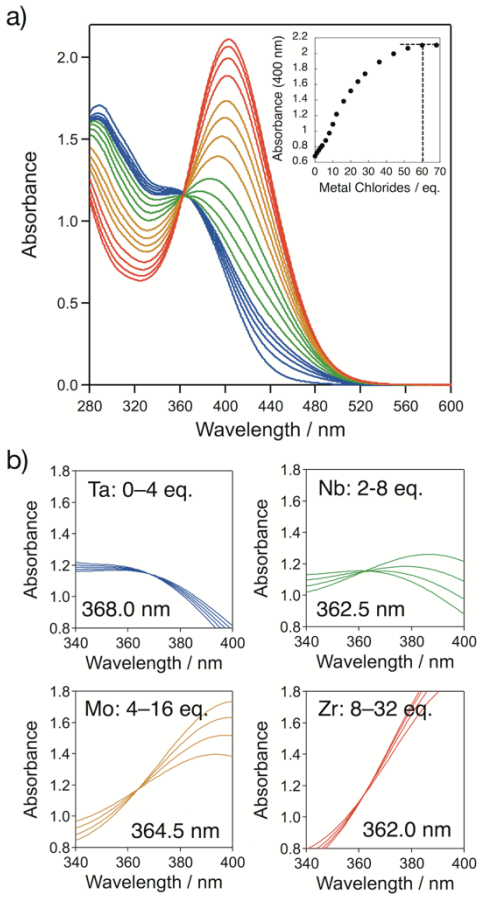

Figure 4. a) Full range (280–600 nm) and b) magnifications around the isosbestic points (340–400 nm) of the UV-vis spectral change of TPM-DPAG4 in CH_2Cl_2/THF = 2/1(*v*/*v*) upon the continuous addition of $TaCl_5$ (0, 1, 2, 3, and 4 eq.; blue lines), $NbCl_5$ (2, 4, 6, and 8 eq.; green lines), $MoCl_5$ (4, 8, 12, and 16 eq.; orange lines), and $ZrCl_4$ (8, 16, 24, and 32 eq.; red lines) in the presence of py (14 eq.) and 3-Clpy (240 eq.) under an atmosphere of N_2 at 245 K. The full spectrum corresponds to the product after the addition of $TaCl_5$ (4 eq.), $NbCl_5$ (8 eq.), $MoCl_5$ (16 eq.), and $ZrCl_4$ (32 eq.).

composition of these metals (Ta/Nb/Mo/Zr = 1/2.6±0.2/4.1±0.2/8.9±0.4), which suggests that the overall content of the metals in the GMC-supported powder sample is consistent with the composition obtained from the titration experiments in solution (Ta/Nb/Mo/Zr = 1/2/4/8). On the other hand, the HAADF-STEM images revealed nanosized assemblies monodispersed on the GMC (Figure S14), and the EDS mapping images show that Ta, Nb, Mo, and Zr are located at the same position in the assemblies (Figures 6 and S15). These results clearly indicate that these four kinds of metals were congregated in the assemblies. Moreover, the peak area of the metals in the EDS spectrum indicated the composition of Ta/Nb/Mo/Zr = 1/1.7±0.2/4.4±0.3/8.3±0.5 (Figures 6b, S16, and Table S2), supporting the defined composition of the heterometallic assembly even in nanoscale. Thus, we clearly demonstrated the first example for the heterometallic assembly that involve four different early 4d/5d-transition metals in a defined composition.

Redox Properties and Formation of Clusters on the Support

Figure 7 shows the XPS spectra of the Mo assembly, of the product of the Mo assembly after the reaction under H_2, and of the product of the heterometallic assembly after the reaction under H_2. Compared to the binding energies (232.2 and 235.5 eV) of Mo^{V} in the Mo assembly, those of the product shifted to lower binding energies (229.0 and 232.3 eV, respectively), suggesting the formation of reduced Mo$^{III–IV}$ species (Figure S17 and Table S3). On the other hand, the product of the heterometallic assembly showed more than two peaks for Mo species (229.5, 232.9, and 236.1 eV). The peak at 229.5 eV was assigned to $3d_{5/2}$ and indicates the existence of reduced Mo$^{III–IV}$ species. The peaks at 232.9 and 236.1 eV were assigned to $3d_{5/2}$ and $3d_{3/2}$, respectively, and thus suggest the presence of oxidized Mo^{VI} species. The $3d_{3/2}$ peak of the reduced Mo species in the product of the heterometallic assembly would be positioned at 232.9 eV and should thus overlap with the $3d_{5/2}$ peak of the oxidized Mo species. These results clearly indicate

that the heterometallic assembly exhibits different redox

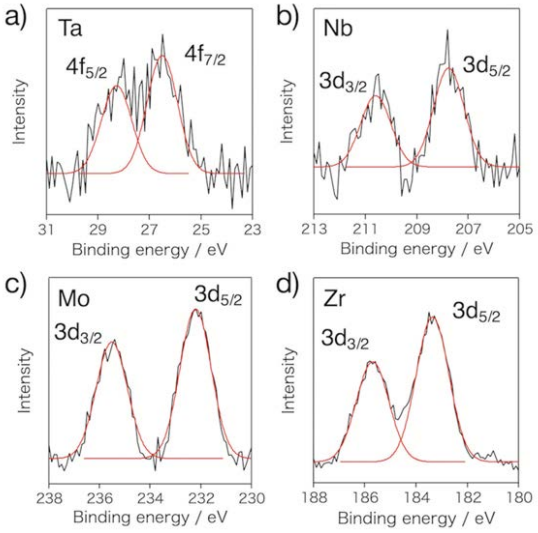

Figure 5. XPS spectra of the assemblies composed of $M^{n+}Cl_n$ (M = Ta^V, Nb^V, Mo^V, Zr^{IV}) and TPM-DPAG4 on the GMC in the range around the binding energies of a) Ta, b) Nb, c) Mo, and d) Zr with fitting curves.

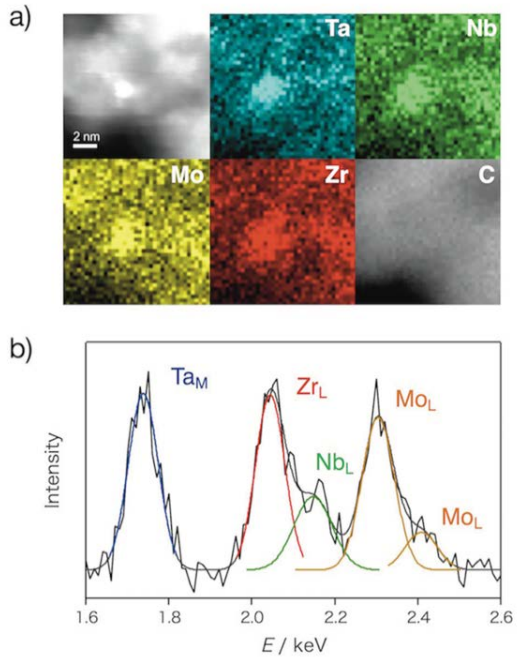

Figure 6. a) HAADF-STEM and EDS mapping images of Ta (light blue), Nb (green), Mo (yellow), Zr (red), and C (grey); b) EDS spectrum on the assembly composed of $M^{n+}Cl_n$ (M = Ta^V, Nb^V, Mo^V, Zr^{IV}) and TPM-DPAG4 on GMC with fitting curves.

properties compared to the Mo assembly. It should also be noted here that the binding energies of Ta (26.7/28.7 eV), Nb (207.7/210.4 eV), and Zr (182.9/185.3 eV) in the product shifted slightly during the reaction, suggesting a change of the coordination environment around these metals (Figure S18 and Table S4). Moreover, a HAADF-STEM image of the product of the heterometallic assembly confirmed the formation of clusters (diameter: 1.2±0.2 nm) dispersed on GMC as shown in Figure 8, demonstrating the application of the heterometallic assembly as a cluster template.

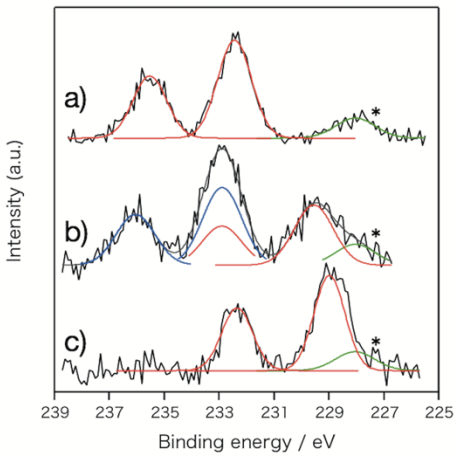

Figure 7. XPS spectra of a) the heterometallic assembly composed of $M^{n+}Cl_n$ (M = Ta^V, Nb^V, Mo^V, Zr^{IV}) and TPM-DPAG4 on GMC; b) the product of the heterometallic assembly after the reaction under an atmosphere of H_2 at 773 K; c) the product of the Mo assembly after the reaction under an atmosphere of H_2 at 773 K; the spectra cover the range of binding energies of Mo with fitting curves. The marked peaks (*) were observed in the GMC.

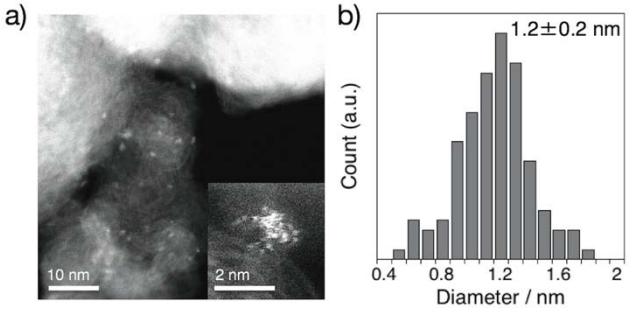

Figure 8. a) HAADF-STEM image and b) size distribution in the product after the reaction of the heterometallic assemblies composed of $M^{n+}Cl_n$ (M = Ta^V, Nb^V, Mo^V, Zr^{IV}) and TPM-DPAG4 on GMC under an atmosphere of H_2 at 773 K. The inset shows a high-resolution image.

Conclusions

This study examined the systematic assembling of the early 4d/5d-transition metals (Zr^{IV}, Nb^V, Mo^V, Hf^{IV}, Ta^V, and W^{VI}) into the TPM-DPAG4 dendrimer by controlling the coordinative interactions between the metals and the imines in the dendrimer. Moreover, the heterometallic assembling of Ta^V, Nb^V, Mo^V, and Zr^{IV} into the TPM-DPAG4 was examined in solution and on the surface of a carbon support. We were thus able to demonstrate for the first time that these heterometallic nanosized assemblies involve four different early 4d/5d-transition metals in a defined composition. These results should provide access to new routes to produce heterometallic nanomaterials that contain the early 4d/5d-transition metals.

Conflicts of interest

There are no conflicts to declare.

Acknowledgements

The authors acknowledge Dr. Ken Albrecht (Kyushu University) for his support with the syntheses of the TPM-DPAG1 and G4 dendrimers. This study was supported by JST ERATO Grant Number JPMJER1503 and JSPS KAKENHI Grant Numbers JP15H05757 and JP18K14237, Japan.

Notes and references

1 B. J. Holliday and C. A. Mirkin, *Angew. Chem. Int. Ed*., 2004, **43**, 2334–2375.
2 S. Kitagawa, R. Kitaura and S.-I. Noro, *Angew. Chem. Int. Ed*., 2004, **43**, 2334–2375.
3 H. N. Miras, J. Yan, D.-L. Long and L. Cronin, *Chem. Soc. Rev*., 2012, **41**, 7403–7430.
4 Z. Luo and A. W. Castleman, *Acc. Chem. Res*., 2014, **47**, 2931−2940.
5 C. G. Granqvist and R. A. Buhrman, *J. Appl. Phys*., 1976, **47**, 2200–2219.
6 F. A. Cotton and T. E. Haas, *Inorg. Chem*., 1964, **3**, 10–17.
7 M. Nippe, G. H. Timmer and J. F. Berry, *Chem. Commun*., 2009, 4357–4359.
8 S. H. Elder, F. M. Cot, Y. Su, S. M. Heald, A. M. Tyryshkin, M. K. Bowman, Y. Gao, A. G. Joly, M. L. Balmer, A. C. Kolwaite, K. A. Magrini and D. M. Blake, *J. Am. Chem. Soc.,* 2000, **122***,* 5138–5146.
9 D. Liu, L. Liu, G. Li and C. Liu, *J. Nat. Gas Chem.,* 2010, **19**, 530–533.
10 J. A. Mendoza-Nieto, O. Vera-Vallejo, L. Escobar-Alarcón, D. Solís-Casados and T. Klimova, *Fuel*, 2013, **110**, 268–277.
11 R. L. Keiter, R. D. Borger, M. J. Madigan, S. L.Kaiser and D. L. Rowley, *Inorg. Chim. Acta,* 1983, **76**, L5–L6.
12 S. Gross, G. Kickelbick, M. Puchberger and U. Schubert, *Monatshefte für Chemie*, 2003, **134**, 1053–1063.
13 E. V. Radkov, V. G. Young Jr. and R. H. Beer, *J. Am. Chem. Soc.,* 1999, **121***,* 8953–8954.
14 E. de Barros Santos, J. M. de Souza e Silva, F. A. Sigoli and I. O. Mazali, *J. Nanopart. Res.,* 2011, **13**, 5909–5917.
15 K. Miyajima, H. Himeno, A. Yamada, H. Yamamoto and F. Mafuné, *J. Phys. Chem. A,* 2011, **115**, 1516–1520.
16 D. A. Tomalia, H. Baker, J. Dewald, M. Hall, G. Kallos, S. Martin, J. Roeck, J. Ryder and P. Smith, *Polym. J.,* 1985, **17**, 117–132.
17 D. A. Tomalia, A. M. Naylor and W. A. Goddard III, *Angew. Chem. Int. Ed*., 1990, **29**, 138–175.
18 L. Balogh and D. A. Tomalia, *J. Am. Chem. Soc.,* 1998, **120***,* 7355–7356.
19 R. M. Crooks, M. Zhao, L. Sun, V. Chechik and L. K. Yeung, *ACC. Chem. Res*., 2001, **34**, 181–190.
20 R. W. J. Scott, O. M. Wilson and R. M. Crooks, *J. Phys. Chem. B,* 2005, **109***,* 692–704.
21 V. C. P. da Costa and O. Annunziata, *Langmuir,* 2017, **33**, 5482−5490.
22 S. Ghosh and A. Saha, *Nanoscale Res. Lett.,* 2009, **4**, 937–941.
23 I. Willerich and F. Gröhn, *Angew. Chem. Int. Ed*., 2010, **49**, 8104–8108.
24 I. Willerich and F. Gröhn, *Chem. Eur. J*., 2008, **14**, 9112–9116.
25 S. Frühbeißer and F. Gröhn, *Macromol. Chem. Phys.,* 2017*,* **218***,* 1600526.
26 P. Bhattacharya, S. H. Kim, P. Chen, R. Chen, A. M. Spuches, J. M. Brown, M. H. Lamm and P. C. Ke, *J. Phys. Chem. C,* 2012, **116**, 15775−15781.
27 K. Baczko, H. Fensterbank, B. Berini, N. Bordage, G. Clavier, R. Méallet-Renault, C. Larpent and E. Allard, *J. Polymer Sci. Polymer Chem.,* 2016, **54**, 115–126.
28 X. Liu, J. Zhou, T. Yu, C. Chen, Q. Cheng, K. Sengupta, Y. Huang, H. Li, C. Liu, Y. Wang, P. Posocco, M. Wang, Q. Cui, S. Giorgio, M. Fermeglia, F. Qu, S. Pricl, Y. Shi, Z. Liang, P. Rocchi, J. J. Rossi and Ling Peng, *Angew. Chem. Int. Ed*., 2014, **53**, 11822–11827.
29 Q. Sun, X. Sun, X. Ma, Z. Zhou, E. Jin, B. Zhang, Y. Shen, E. A. Van Kirk, W. J. Murdoch, J. R. Lott, T. P. Lodge, M. Radosz and Y. Zhao, *Adv. Mater*., 2014, **26**, 7615–7621.
30 Q. Sun, X. Ma, B. Zhang, Z. Zhou, E. Jin, Y. Shen, E. A. Van Kirk, W. J. Murdoch, M. Radosz and W. Sun, *Biomater. Sci*., 2016, **4**, 958–969.
31 Y. Li, X. Xu, X. Zhang, Y. Li, Z. Zhang and Z. Gu, *ACS Nano,* 2017, **11**, 416−429.
32 K. Yamamoto, M. Higuchi, S. Shiki, M. Tsuruta and H. Chiba, *Nature,* 2002, **415**, 509–511.
33 K. Yamamoto, T. Imaoka, W.-J. Chun, O. Enoki, H. Katoh, M. Takenaga and A. Sonoi, *Nat. Chem*., 2009, **1**, 397–402.
34 K. Yamamoto and T. Imaoka, *Bull. Chem. Soc. Jpn*., 2006, **79**, 511–526.
35 K. Yamamoto and K. Takanashi, *Polymer,* 2008, **49**, 4033–4041.
36 K. Yamamoto and T. Imaoka, *Acc. Chem. Res*., 2014, **47**, 1127–1136.
37 K. Albrecht, N. Sakane and K. Yamamoto, *Chem. Commun.,* 2014, **50**, 12177–12180.
38 K. Takanashi, A. Fujii, R. Nakajima, H. Chiba, M. Higuchi, Y. Einaga and K. Yamamoto, *Bull. Chem. Soc. Jpn*., 2007, **80**, 1563–1572.
39 M. Takahashi, H. Koizumi, W.-J. Chun, M. Kori, T. Imaoka and K. Yamamoto, *Sci. Adv*., 2017, **3**, 1–8, e1700101.
40 N. Satoh and K. Yamamoto, *Synth. Met*., 2009, **159**, 813–816.
41 R. G. Pearson, *J. Am. Chem. Soc.,* 1963, **85**, 3533–3539.
42 K. Takanashi, H. Chiba, M. Higuchi and K. Yamamoto, *Org. Lett.,* 2004, **6**, 1709–1712.
43 O. Enoki, H. Katoh and K. Yamamoto, *Org. Lett*., 2006, **8**, 569–571.
44 F. Cataldo, *Eur. Chem. Bull.,* 2015*,* **4***,* 92–97.
45 K. A. Connors, *Binding constants: the measurements of molecular complex stability*, John Wiley + Sons, 1987.
46 G. H. Cartledge, *J. Am. Chem. Soc*., 1928, **50**, 2855–2863.
47 R. D. Shannon, *Acta. Cryst.,* 1976, **A32**, 751–767.
48 T. Hiraoki, M. Kaneko and K. Hikichi, *Polym. J*., 1979, **11**, 397–403.
49 S. Balt, M. W. G.de Bolster and G.Visser-Luirink, *Inorg. Chim. Acta,* 1983, **3**, 121–127.
50 D. Augustin-Nowacka and L. Chmurzyñski, *Anal. Chim. Acta,* 1999, **381**, 215–220.

Heterometallic Nanosized Assembling of Early 4d/5d-transition Metal Ions into TPM-DPAG4 Dendrimer